Enhanced Normal Zone Propagation Velocity in REBCO Coated Conductors Using an Intermetallic Stabilizer Coating

P. Barusco, H. Ben-Saad, D. Horn-Bourque, C. Lacroix, F. Sirois, *Senior Member, IEEE*, T. Puig, J. Gutiérrez, X. Granados, *Member, IEEE*, and X. Obradors, *Senior Member, IEEE*

(Invited Paper)

***Abstract*—The Current Flow Diverter (CFD) is an established concept that has proven to effectively reduce the probability of destructive hot spots by boosting the normal zone propagation velocity (NZPV) in commercial $REBa_2Cu_3O_7$ (REBCO; RE = Rare Earth) coated conductors (CC). However, incorporating the CFD concept requires finding a scalable method that is also compatible with the already established R2R fabrication process used by CC manufacturers. This study presents a new simple & cost-effective proof-of-concept technique capable of recreating the CFD architecture in commercial CCs coated with silver. The technique is based on promoting a locally controlled thin film diffusion reaction between the silver stabilizer and pure indium. Due to fast diffusion in the Ag-In system, stable Intermetallic Compounds (IMC) are formed throughout the whole thickness of the silver layer reaching the REBCO interface. The presence of Ag-In IMC in the interface safely increases the interfacial resistance (Ω-cm^2) by orders of magnitude, thus allowing to safely form the CFD interlayer. Silver-coated tape samples altered using this CFD-IMC have shown an NZPV increase of 5–8x when compared with pristine samples.**

***Index Terms*—Coated conductors, HTS, NZPV, quench.**

Manuscript received 25 September 2023; revised 29 December 2023; accepted 31 December 2023. Date of publication 23 January 2024; date of current version 8 February 2024. This work was supported in part by the FASTGRID Project under Grant EUH2020-721019, in part by the Projects SUPERENERTECH under Grant PID2021-127297OB-C21, in part by Spanish Ministry of Economy and Competitiveness which were co-funded by the European Regional Development Fund through SUMATE under Grants RTI2018-095853-BC21 and RTI2018-095853-B-C22, in part by the MCIN/AEI/10.13039/501100011033 and EU "NextGenerationEU"/PRTR through SUPERPOWER Project under Grant TED2021-130004B-I00, in part by the Generalitat de Catalunya under Grant 2017-SGR 753, and in part by the COST Action NANOCOHYBRI under Grant CA16218. The work of P. Barusco, T. Puig, X. Granados, J. Guriérrez and X. Obradors was supported by the Center of Excellence Awards Severo Ochoa under Grants SEV-2015-0496 and CEX2019-000917-S. *(Corresponding authors: X. Obradors; P. Barusco.)*

P. Barusco, T. Puig, J. Gutiérrez, X. Granados, and X. Obradors are with the Campus de la UAB, Institut de Ciència de Materials de Barcelona (ICMAB-CSIC), 08193 Bellaterra, Spain (e-mail: pbarusco@icmab.es; teresa.puig@icmab.es; jgutierrez@icmab.es; granados@icmab.es; xavier.obradors@icmab.es).

H. Ben-Saad, D. Horn-Bourque, C. Lacroix, and F. Sirois are with the Polytechnique Montréal, Montréal QC H3T 1J4, Canada (e-mail: haifa.ben-saad@polymtl.ca; delano.horn-bourque@polymtl.ca; c.lacroix@polymtl.ca; f.sirois@polymtl.ca).

Color versions of one or more figures in this article are available at https://doi.org/10.1109/TASC.2024.3357444.

Digital Object Identifier 10.1109/TASC.2024.3357444

I. Introduction

THE second generation (2G) of high-temperature superconductor (HTS) tapes, i.e., coated conductors (CCs, also known as "HTS tapes"), is currently the most promising wire architecture capable of incorporating the high-performance aspects of superconducting materials in electrical devices such as motors, generators, transmission cables, high-field magnets [1], [2], [3] and superconducting fault current limiters (SFCLs) [4], [5], [6]. However, the "hot spot" regime is a well-known inherent issue of the tape's architecture that hinders its reliable continuous operation. On the condition that the operational current in the tape is near the average critical current (I_c) of the conductor, zones with I_c dropouts [7] can locally (lengthwise) quench [8], i.e., they can switch from the superconducting state to the resistive normal state. If the current in the conductor is not limited quickly enough, a slow thermal propagation of the local quench, also referred to as normal zone propagation velocity (NZPV) [9], [10], is likely to irreversibly damage the tape [11].

The Current Flow Diverter (CFD) is a concept that has proven to increase the NZPV by about one order of magnitude and reduce the probability of a destructive *hot spot* scenario [12]. This effect is safely achieved by increasing the interfacial resistance Ag/REBCO ρ_c (Ω-cm^2) along the CC's length [9] solely in the middle of its width (95-98% width-wise), thus allowing the global interfacial resistance to be kept low enough ($\sim 10^{-7}$ Ω-cm^2) for installing current terminals or joints of practical sizes (1-10 cm length-wise). In the original CFD proof-of-concept method [12], ρ_c is increased by exposing the REBCO film to the moist ambient atmosphere; the upper silver layer (REBCO side) is partially removed using an etchant solution (NH_4OH: H_2O_2: H_2O 1: 1: 4) and then re-sputtered. Although effective and simple to reproduce on a small scale (10-100 cm), the waste of expensive silver material remains undesirable and finding an alternating route that is simpler and less costly would help to promote the production of kilometers of CFD-CCs.

In 2021, a method based on the Reactive Co-evaporation and Cyclic Deposition Reaction (RCE-CDR) of Cerium Oxide (CeO_2) was proposed for CCs from STI Inc. to form the CFD layer (Ag/CeO_2/REBCO) [13]. Unfortunately, the reactivity of the CeO_2 with the REBCO at the interface during the

$REBa_2Cu_3O_{7-\delta}$ oxygen annealing process [14], [15], [16], led to a drastic degradation of the superconducting properties [13]. One year later, another method using the Chemical Solution Deposition (CSD) of amorphous Yttrium Oxide (Y_2O_3) was successfully tested on *THEVA GmbH* CCs to form a CFD structure Ag/Y_2O_3/REBCO. However, the oxygenation of the REBCO film in the presence of the yttria-CFD layer could only be accomplished by inserting an intermediate extra step into the standard fabrication process [17], which would compromise the industry's throughput goals. Most recently, a novel approach was proposed based on a partial transformation of the Ag layer into Ag_2S to reach the so-called buffer-layer-CFD (bCFD) CC architecture, which also considerably enhances the NZPV [18]. Although cost-effective, this approach requires using a sulfurization technique that is yet new to the R2R systems of CC manufactures.

So far, all these near CFD attempts indicate that the most convenient method would be one that avoids altering the two last steps of the standard CC's fabrication: silver deposition and oxygen annealing (oxygenation). Conveniently, a common problem described by authors as "bad contact materials" seems to arise as a solution to by-pass these steps. For instance, if non-noble metals like lead, indium, tin, chromium, nickel and copper are directly deposited onto the REBCO film, they form oxide compounds by reacting with the oxygen at the REBCO interface, thus creating impractical contact pads with high ρ_c. Ekin et al. explained this problem as an interfacial chemistry issue related to high oxygen affinity [19] and showed in [20] that In2%Ag solder, when applied directly to samples of bulk YBCO, forms a resistive indium oxide layer at the interface. Moreover, due to the tendency of metals of Group 11 (e.g., Ag) to quickly diffuse into metals of Group 13 and 14 (e.g., In, Sn, Pb, Ga), soldering joints on silver-coated CCs is a very risky and difficult procedure. Once melted, solders containing Sn and In can rapidly consume the thin silver stabilizer layer and harmfully react with the HTS film. Canavan et al. reported on how melted In3%Ag solder rapidly diffuses into the thin silver stabilizer film of standard CCs and can form continuous intermetallic compound (IMC) phases in contact with the REBCO film that causes cracks and considerably increases ρ_c [21].

In this paper, we present a new & simple proof-of-principle to achieve the classic CFD architecture. The method consists of promoting a controlled solid-state reaction of the silver stabilizer layer on a standard CC with another metal, in our case pure indium (In), to create a chemically stable Ag–In IMC phase in the Stabilizer/REBCO interface capable of selectively increasing ρ_c.

II. Experimental Method

The Ag-In binary system was well described by Campbell et al. [22] and the thin film fast reaction of the bilayer Ag–In is a known phenomenon used extensively in the microelectronics packaging industry for producing high melting temperature ($T > 400$ °C) joints from low temperatures soldering procedures [23]. At room temperature (RT), three known stable IMCs can exist in the Ag–In system:

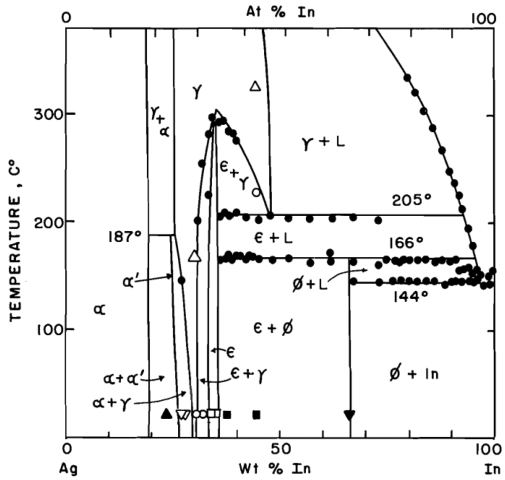

Fig. 1. Phase diagram of the Ag-In system below 300 °C: ▽ $\alpha + \gamma$; ○, $\varepsilon + \gamma$; □, ε; ■, $\varepsilon + \phi$; ▲, $\alpha + \alpha$' (γ-phase metastable). Figure adapted from campbell et al. [22].

- γ-phase: composition Ag3In with hexagonal lattice. The homogeneity ranges from 29 wt % to 29.7 wt % In. The solid solution of Ag + In α-phase ranges bellow 20 wt %.
- ε-phase: composition Ag9In4 (a.k.a Ag2In) with cubic lattice. The homogeneity ranges from 32.8 wt % to 36.82 wt % In; This phase exists together with the γ-phase from 29.7 wt % to 32.8 wt % In.
- ϕ-phase: composition AgIn2 with body-centered tetragonal lattice. This phase exists together with the ε-phase from 36.8 wt % up to 67 wt% In, as well as with pure indium in the case of more than 67 wt % indium in the alloy.

The solid-state diffusion reaction performed in air atmosphere of the bilayer Ag–In follows two main kinetic regimes. The first regime corresponds to the formation of the IMC $AgIn_2$ at the Ag/In interface as soon as the indium is deposited onto the silver (or vice versa). Silver rapidly diffuses through the $AgIn_2$ interface towards the pure In and only $AgIn_2$ grows as long as the pure indium layer has not been fully consumed in the reaction. The diffusion coefficient D in this first regime is found to be in 10^{-15} to 10^{-13} cm^2/s range at RT [24]. Once the Indium is completely consumed, the second regime starts: from the remaining $AgIn_2$ and the excess Ag, IMC Ag_2In starts forming near the interface $Ag/AgIn_2$ and at the silver grain boundaries. The Ag_2In grows more slowly ($D \sim 10^{-16}$ to 10^{-15} cm^2/s at RT) with ageing until all $AgIn_2$, or all the Ag base layer, is consumed [24]. Even though working with the ϕ-phase in the first regime would result in faster diffusion rates at RT, the high ductility of the $AgIn_2$ compound makes it unsuitable to be used as the CC's stabilizer/shunt. Given that the growth rate of the Ag_2In phase drastically increases with temperature ($D \sim 10^{-11}$ cm^2/s at 150 °C) our best option is forming Ag_2In at the REBCO interface using a low temperature annealing process in ambient atmosphere. A second advantage of using Ag_2In instead of $AgIn_2$ is that the higher melting temperature (> 200 °C) of this phase results in better chemical stability for occasional soldering procedures.

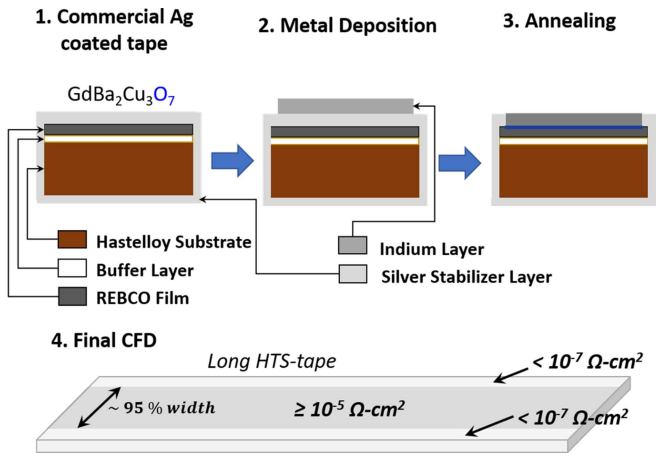

Fig. 2. Sequence of procedures for creating the CFD-IMC architecture. Only two steps required for silver-coated HTS tapes: metal deposition and low-temperature annealing (<200 °C).

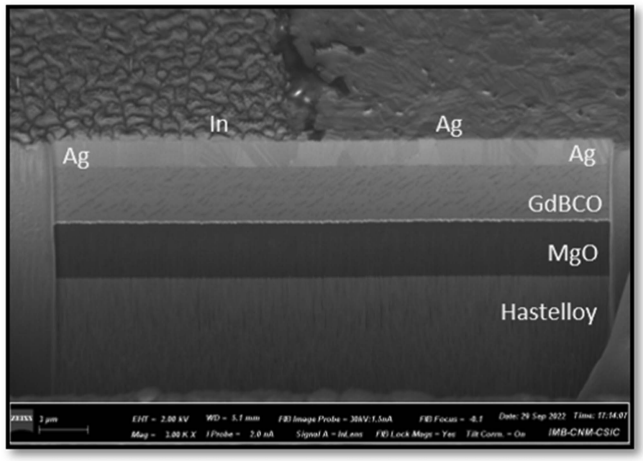

Fig. 3. Cross sectional SEM-FIB image of a THEVA tape used as template for the CFD-IMC method showing the layers Ag/GdBCO/MgO/Hastelloy. The FIB cut was taken after indium evaporation, in the boundary region between Ag-In and In-free Ag at the edges of the tape.

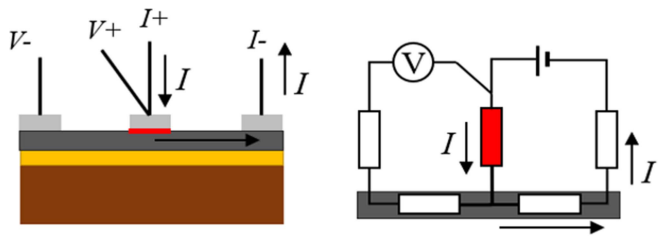

Fig. 4. Three-terminal (3T) configuration for measuring the interfacial resistance in the REBCO coated conductor samples.

Therefore, as illustrated in Fig. 2, by selectively depositing pure indium in the middle width of a silver-coated CC with an appropriate thickness, a new metal stabilizer layer composed primarily of Ag_2In, can be created by annealing the In-Ag system in ambient atmosphere.

A. HTS Tapes & CFD Preparation

In this work, all REBCO CC samples came from a reel-to-reel manufacturing unit produced by THEVA [25]. The CC was built on a 100 μm thick electropolished Hastelloy substrate, where a 3 µm thick texturized layer of MgO was evaporated using an inclined deposition technique (ISD) [26]. A second 450 nm thick layer MgO was deposited at a perpendicular angle to serve as cap coating. The GdBCO HTS was grown as a 3 µm thick layer on top of the MgO via electron beam evaporation from a granulate [25], [27]. Finally, the tape was encapsulated by a 1.3–1.5 µm thick silver layer deposited via electron beam (E-beam) evaporation.

Tape samples with these pristine layers, Ag/GdBCO/MgO/Hastelloy, were used as template for testing CFD fabrication methods. Indium layers of ~800 nm were deposited using an E-beam evaporator manufactured by AJA International Inc. Model ATC-8E Orion, equipment with 10kV HV source from Telemark. The source pellets of 99.999% indium were acquired from Neyco. The cross-sectional SEM-FIB image shown in Fig. 3 illustrates the final stack of layers after the indium deposition and annealing.

B. Interfacial Resistance and NZPV Measurements

A three-terminal (3T) sensing technique was used for measuring the resistance of the interface between the GdBCO layer and the metal stabilizer (either pure Ag or Ag–In intermetallic) in CC samples. Samples were produced by manually cutting sections of larger 12 mm-wide tapes into smaller 5 × 12 mm pieces. Afterwards, the sample pieces were spin-coated with a photoresist solution, patterned in a photolithography machine and chemically etched to create the metal pads/electrodes needed for the 3T measurements (Fig. 4). The imprinted pads were circular in shape with a diameter of 0.7 mm. The etching was accomplished with a NH_4OH: H_2O_2: H_2O solution in the case of the pristine & classic-CFD samples containing layers of pure silver, and a solution of HNO_3: H_2O solution for the CFD-IMC samples containing layers of indium-silver alloys.

After etching, the samples were mounted on a sample holder (a.k.a. transport puck) and measured in a commercial PPMS system from *Quantum Design*. An ultrasonic wired bonder was used to make the terminals with 25 µm diameter aluminum wires via wedge bonding. The small thermal mass of the chosen thin Al wire allows bonding at RT with and firm weld onto the metal stabilizer surface without exposing the stabilizer-REBCO interface to temperatures spikes.

In the 3T configuration illustrated in Fig. 4, for $T < T_c$, the bulk resistance of the REBCO films is essentially by-passed by having one of the pads used for current, common to one of the pads used for voltage reading, thus isolating the measured resistance to the sum of the metal-pad/REBCO interface plus the bulk resistance of the common pad (central pad). Given the dimensions of the central pad and its materials' resistivity (pure Ag or Ag-In IMC), the pad's bulk resistance can be neglected leaving us with the interfacial resistance. In this configuration, the R(T) curves was measured from 300 to 60 K with a current

of 20 $mA_{pk\text{-}pk}$ at 10 Hz. The final ρ_c(T) was calculated by multiplying R(T) by the area of the common/central pad.

The NZPV was measured with a homemade pulsed transport current system using 12 cm long tape samples [28]. Tailored sample holders, built with standard PCB boards, were used to probe 38 differential voltage signals lengthwise on the REBCO-stabilizer side of the tape. A cylindrical NdFeB magnet was also positioned in the middle of tape to reduce the critical current locally and induce the initial quench in the region under the array of voltage probes.

The NZPV tests were performed by immersing the arrangement, holder and sample, into a liquid nitrogen bath. Once thermal stabilization was reached, current pulses of 5–30 ms and amplitude close to the I_c of the tape were applied. The quench was initiated in the region under the NdFeB magnet and the propagation of the quench in time was evaluated using an 80-channels data acquisition card from National Instruments to record the voltage drops across the array of probes. The final NZPV value as a function of current amplitude was calculated by considering the time delay between probes to reach an arbitrary voltage threshold. A more detailed description of this system can be found in [28].

C. Microstructural Characterization

X-ray diffraction patterns of the samples were obtained using a general area detector GADDS diffractometer (Bruker-AXS model D8) equipped with a 2D detector and Cu Kα radiation. The different stacked thin-film layers were analyzed for morphology and the chemical composition was determined using a dual beam (SEM-FIB) Zeiss 1560 XB apparatus for taking FIB cross-section images.

III. Results

Four main pieces of commercial silver-coated GdBCO tape were cut from the main reel; two of 5 cm length, sample #1 and #4, and two of 12 cm length, samples #2 and #3. Sample #4 was fully altered using the classic-CFD method of etching and re-sputtering the silver layer along the middle width of the tape as described in [12]. Assuming a homogenous thickness of 1.4 µm silver layer as shown in Fig. 3, sample #1 was evaporated with enough indium to achieve full ε-phase at 40 wt % in indium weight. The XRD analysis of sample #1, performed 48 h after evaporation, reveals an absence of pure indium in the θ–2θ scan taken at RT. Only large amounts of ϕ-phase and some ε-phase were seen, meaning that all indium, as deposited, was consumed in the reaction with the silver layer (in 48 h at RT) to form $AgIn_2$.

Another 5 × 12 mm piece, sample #1.1, was cut from the as-deposited sample #1, and annealed for a couple of hours at low temperature (< 200 °C, for instance 160 °C) in ambient air. After annealing, the absence of the two main silver peaks (111) and (200) in the $\theta-2\theta$ scan of Fig. 5 indicates that all the silver was consumed to form the desired ε-phase, leaving some ϕ-phase residue.

To confirm the presence of the silver-indium IMC in the interface of the GdBCO film, another 5 mm piece, sample #1.2, was cut and annealed in the same conditions as sample #1.1. Afterwards, using the SEM-FIB system, a 1 × 10 × 10 µm lamella was taken from sample #1.2 to analyze the In-Ag/GdBCO/MgO layers. A Pt cap layer was deposited on top of the In-Ag layer to allow the extraction of the lamella using a microneedle for further EDS analysis. Fig. 6 reveals two phases in the Ag-In layer: the pure ε-phase, in contact with the GdBCO, and some residual ϕ-phase regions on top. This conclusion is reinforced by the EDS-mapping shown in Fig. 7 where traces of indium and silver were found in the same regions following the same distribution profile along the interface with the GdBCO layer.

The possibility of indium diffusion into the GdBCO layer was also verified by extracting the lamella shown in Fig. 7 and milling it locally to reduce its thickness. The thickness was trimmed from 1 µm down to ∼100 nm and a single EDS line was taken across the Ag-In/GdBCO interface using a 10 kV excitation for the electron beam. As shown in Fig. 8 , as the EDS line crosses the GdBCO region towards the Ag-In layer, the counts for indium and silver sharply appear together in the

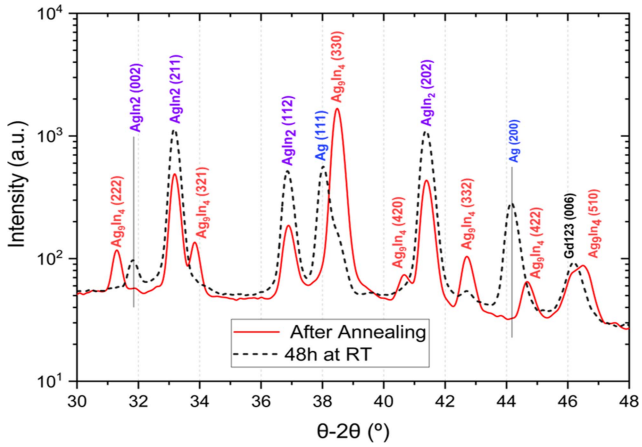

Fig. 5. X-ray diffraction spectra of the Ag-In layers on top of the silver layer shunt of a GdBCO coated conductor after 48 h at RT, after annealing at low temperature.

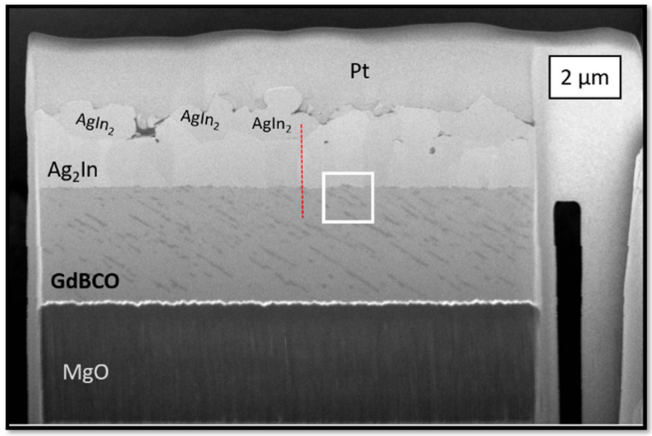

Fig. 6. SEM-FIB image of the lamella taken from sample #2, showing the layers In-Ag/GdBCO/MgO after air annealing. The red dashed line represents the path used for an EDS line analysis. The white box represents the chosen region for the EDS mapping.

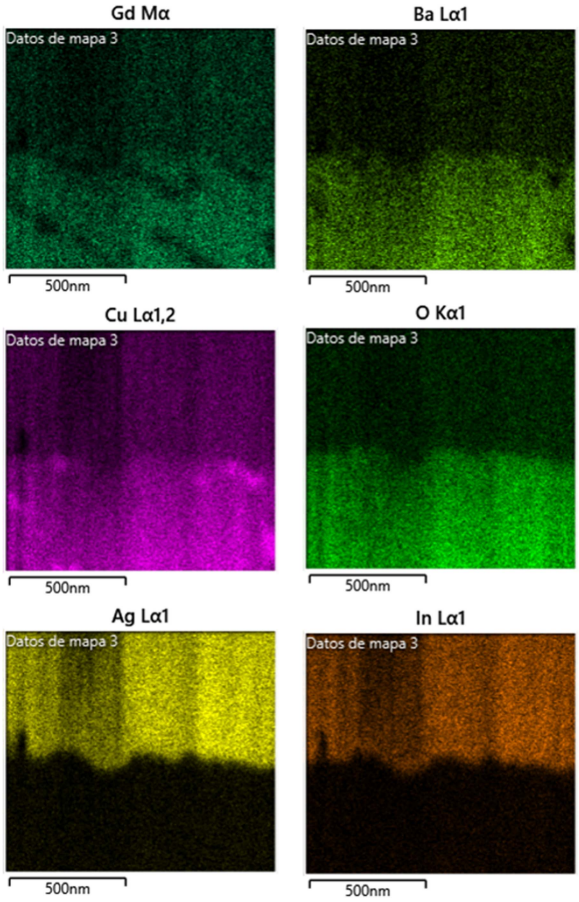

Fig. 7. SEM image of the In-Ag/GdBCO interface. The white square of Fig. 6 indicates the zone where the EDS mapping was performed. The EDS maps reveal the elements present in the composition of the sample.

correct proportion to correspond to the ε-phase. Above a distance of 2.5 µm in the EDS line, the Ag/In proportion corresponds to the ϕ-phase residue. Small traces of oxygen and barium were found in a very narrow region of the GdBCO interface ($\sim$20 nm) thus allowing us to consider the occurrence of harmful indium diffusion insignificant.

Two more samples, #1.3 and #1.4, were taken from the parent-sample #1 and annealed in the same conditions than sample #1.1. Both were tested for their interfacial resistance (ρ_c) as a function of temperature using the procedure described in Section II-B. In Fig. 9, a comparison of the experimental ρ_c curves of both samples against a pristine-THEVA sample and a classic-CFD, sample #4, reveals a profile closer to that of the classic-CFD; below the critical temperature ($T < 92$ K), ρ_c remains above 10^{-5} Ω-cm^2 instead of dropping orders of magnitude like in the case of the pristine THEVA tapes.

Following the confirmation of the increase of ρ_c due to the presence of the silver-indium IMC at the GdBCO interface, samples #2 and #3 were also exposed to pure indium evaporation and annealed using the same procedure as in sample #1. Both samples were tested for the NZPV using the transport current system described in Section II-B. The results shown in

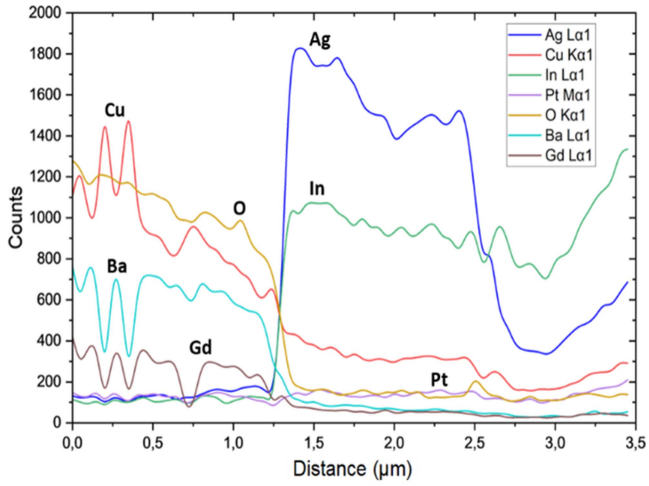

Fig. 8. EDS line profiles across the In-Ag/GdBCO interface for the milled lamella taken from sample #2 and shown in Figs. 6 and 7.

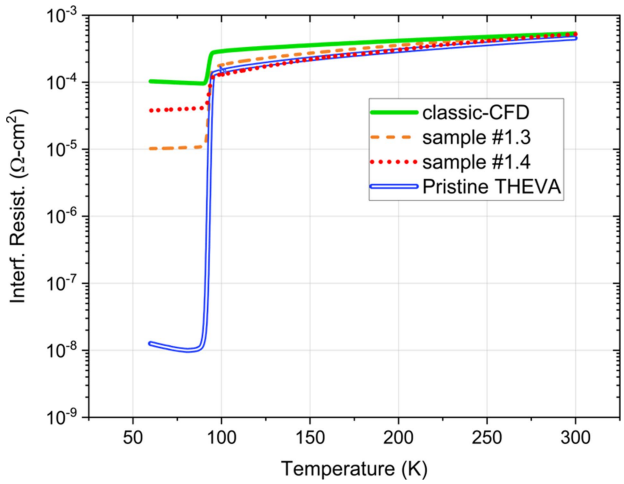

Fig. 9. Experimental interfacial resistance $\boldsymbol{\rho_c}$ versus temperature for samples #2.1 and #2.2, obtained for the 60 × 300 K range in self-field.

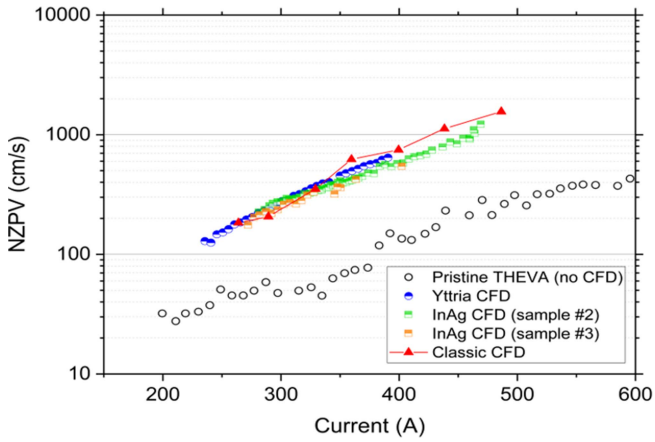

Fig. 10. Experimental NZPV obtained at 77 K in self-field (symbols) versus applied current for all samples. Results for the classic CFD, Yttria CFD and pristine THEVA (i.e., no CFD) samples were taken from the FASTGRID project [17], [29].

Fig. 10 reveal a consistent 5–8x increase in the NZPV for both indium-altered samples. These values are very close to the ones measured during the FASTGRID project, where classical CFD samples were made with silver-coated tapes from THEVA [29] as well as coated conductors with an insulating Yttria layer with the CFD geometry [17], [29].

IV. Conclusion

A new method to create silver-coated CCs with the CFD architecture has been proposed and successfully tested. Thin film layers of indium were evaporated onto the silver-stabilizer of commercial HTS tape samples, selectively covering 95-98% of their middle section. The samples were subsequently annealed in air at low-temperature (< 200 °C) to promote a fast thin-film Ag-In interdiffusion reaction. Post-annealing XRD analysis revealed that the full silver reacted with the indium to form an Ag-In IMC, namely ε-phase (Ag_9In_4) SEM-FIB cross-section images of the layers Ag-In/GdBCO/MgO confirmed the integrity of the GdBCO film in the presence of the ε-phase at the REBCO surface. Three-terminal transport measurements taken for indium-altered-samples confirmed a significant increase of the interfacial resistance ($\rho_c > 10^{-5}\,\Omega$-cm^2) in the 60-92 K temperature range, similar to that observed in classical CFD samples. Finally, the NZPV tests performed on two 12 cm indium-altered tape samples indicated a substantial increase in the quench velocity, namely a 5-8x gain when compared to pristine silver-coated THEVA tapes.

The authors believe that the use of indium to create the CFD is an extremely appealing approach given its simplicity and convenience regarding the steps in R2R fabrication. Indeed, i) the low annealing temperature avoids I_c degradation in the REBCO film, ii) the short annealing time should not compromise tape throughput, and iii) the metal-deposition is an already well-established technique. Currently, indium as a raw material is 3x cheaper than silver, but this extra cost should be taken into account for the CC final price. Substituting In for a cheaper metal like tin (Sn) or zinc (Zn) is an alternative that will be investigated in future work. Reducing the cost by decreasing the amount of the deposited indium and forming γ-phase (Ag_3In) at the REBCO interface instead of ε-phase is also an option currently under investigation.

References

[1] X. Obradors and T. Puig, "Coated conductors for power applications: Materials challenges," *Supercond. Sci. Technol.*, vol. 27, no. 4, Apr. 2014, Art. no. 044003.

[2] J. L. MacManus-Driscoll and S. C. Wimbush, "Processing and application of high-temperature superconducting coated conductors," *Nature Rev. Mater.*, vol. 6, no. 7, pp. 587–604, Jul. 2021.

[3] T. Puig, J. Gutierrez, and X. Obradors, "Impact of high growth rates on the microstructure and vortex pinning of high-temperature superconducting coated conductors," *Nature Rev. Phys.*, to be published, doi: 10.1038/s42254-023-00663-3.

[4] P. Tixador, *Book: Superconducting Fault Current Limiter*, vol. 3. Singapore: World Scientific, 2018.

[5] P. Tixador et al., "Status of the European union project FASTGRID," *IEEE Trans. Appl. Supercond.*, vol. 29, no. 5, Aug. 2019, Art. no. 5603305.

[6] M. Moyzykh et al., "First Russian 220 kV superconducting fault current limiter (SFCL) for application in city grid," *IEEE Trans. Appl. Supercond.*, vol. 31, no. 5, Aug. 2021, Art. no. 5601707.

[7] M. Lao, J. Bernardi, M. Bauer, and M. Eisterer, "Critical current anisotropy of GdBCO tapes grown on ISD–MgO buffered substrate," *Supercond. Sci. Technol.*, vol. 28, no. 12, Dec. 2015, Art. no. 124002.

[8] A. Gurevich, "Thermal instability near planar defects in superconductors," *Appl. Phys. Lett.*, vol. 78, no. 13, pp. 1891–1893, Mar. 2001.

[9] G. A. Levin, K. A. Novak, and P. N. Barnes, "The effects of superconductor–stabilizer interfacial resistance on the quench of a current-carrying coated conductor," *Supercond. Sci. Technol.*, vol. 23, no. 1, Jan. 2010, Art. no. 014021.

[10] M. Bonura and C. Senatore, "An equation for the quench propagation velocity valid for high field magnet use of REBCO coated conductors," *Appl. Phys. Lett.*, vol. 108, no. 24, Jun. 2016, Art. no. 242602.

[11] A. Kudymow, M. Noe, C. Schacherer, H. Kinder, and W. Prusseit, "Investigation of YBCO coated conductor for application in resistive superconducting fault current limiters," *IEEE Trans. Appl. Supercond.*, vol. 17, no. 2, pp. 3499–3502, Jun. 2007.

[12] C. Lacroix and F. Sirois, "Concept of a current flow diverter for accelerating the normal zone propagation velocity in 2G HTS coated conductors," *Supercond. Sci. Technol.*, vol. 27, no. 3, Mar. 2014, Art. no. 035003.

[13] J. H. Fournier-Lupien, C. Lacroix, J. Huh, J. P. Masse, J. Bellemare, and F. Sirois, "Effect of annealing on HTS tapes with a cerium oxide layer inserted between the REBaCuO and silver layers," *Materialia*, vol. 15, 2021, Art. no. 101029.

[14] Y. Ikuma and S. Akiyoshi, "Diffusion of oxygen in $YBa_2Cu_3O_{7-y}$," *J. Appl. Phys.*, vol. 64, no. 8, pp. 3915–3917, Jun. 1998.

[15] H. S. Kim et al., "The influence of heat-treatment and oxygenation annealing on the superconducting properties of YBCO coated conductors," *Supercond. Sci. Technol.*, vol. 22, no. 12, Dec. 2009, Art. no. 125016.

[16] P. Cayado et al., "Untangling surface oxygen exchange effects in $YBa_2Cu_3O_{6+x}$ thin films by electrical conductivity relaxation," *Phys. Chem. Chem. Phys.*, vol. 19, no. 21, pp. 14129–14140, 2017.

[17] P. Barusco et al., "Chemical solution deposition of insulating yttria nanolayers as current flow diverter in superconducting $GdBa_2Cu_3O_{7-\delta}$ coated conductors," *Amer. Chem. Soc. Omega*, vol. 7, no. 18, pp. 15315–15325, May 2022.

[18] P. Barusco et al., "A sulfurization method for creating the buffer-layers current flow diverter architecture in $REBa_2Cu_3O_7$ coated conductors," *Supercond. Sci. Technol.*, vol. 36, no. 12, Dec. 2023, Art. no. 125005.

[19] J. W. Ekin, A. J. Panson, and B. A. Blankenship, "Method for making low-resistivity contacts to high T_c superconductors," *Appl. Phys. Lett.*, vol. 52, no. 4, pp. 331–333, Jan. 1988.

[20] J. W. Ekin et al., "High T_c superconductor/noble-metal contacts with surface resistivities in the $10-10\,\Omega$ cm^2 range," *Appl. Phys. Lett.*, vol. 52, no. 21, pp. 1819–1821, May 1988.

[21] E. R. Canavan, H. Leidecker, and L. Panashchenko, "Conductance degradation in HTS coated conductor solder joints," *IOP Conf. Ser. Mater. Sci. Eng.*, vol. 102, no. 1, 2015, Art. no. 012032.

[22] A. N. Campbell, R. Wagemann, and R. B. Ferguson, "The silver–indium system: Thermal analysis, photomicrography, electron microprobe, and X-Ray powder diffraction results," *Can. J. Chem.*, vol. 48, no. 11, pp. 1703–1715, Jun. 1970.

[23] R. W. Chuang and C. C. Lee, "Silver-indium joints produced at low temperature for high temperature devices," *IEEE Trans. Compon. Packag. Technol.*, vol. 25, no. 3, pp. 453–458, Sep. 2002.

[24] P. J. Rossi, N. Zotov, and E. J. Mittemeijer, "Kinetics of intermetallic compound formation in thermally evaporated Ag-In bilayers," *J. Appl. Phys.*, vol. 120, no. 16, Oct. 2016, Art. no. 165308.

[25] W. Prusseit, R. Nemetschek, C. Hoffmann, G. Sigl, A. Lümkemann, and H. Kinder, "ISD process development for coated conductors," *Phys. C Supercond. Appl.*, vol. 426–431, pp. 866–871, Oct. 2005.

[26] R. Metzger, M. Bauer, K. Numssen, R. Semerad, P. Berberich, and H. Kinder, "Superconducting tapes using ISD buffer layers produced by evaporation of MgO or reactive evaporation of magnesium," *IEEE Trans. Appl. Supercond.*, vol. 11, no. 1, pp. 2826–2829, Mar. 2001.

[27] S. S. Oh et al., "Progress in research and development for REBCO coated conductors by reactive co-evaporation," *Supercond. Cryog*, vol. 15, no. 4, pp. 1229–3008, Dec. 2013.

[28] J. Giguère et al., "High normal zone propagation velocity in copper-stabilized 2G HTS coated conductors," *Supercond. Sci. Technol.*, vol. 34, no. 4, Apr. 2021, Art. no. 045010.

[29] C. Lacroix et al., "Normal zone propagation in various REBCO tape architectures," *Supercond. Sci. Technol.*, vol. 35, no. 5, May 2022, Art. no. 055009.